JMEPEG (1993) 2:671-682

Intelligent Control of Consolidation and Solidification Processes*

N.M. Wereley, T.F. Zahrah, and F.H. Charron

Intelligent processing of materials (IPM) deals with the integration of process models and *in situ* sensors into an intelligent process controller to achieve desired material properties. IPM-based control systems recently have been developed for both consolidation and solidification processes. This article explores the application of models based on the finite-element method (FEM) to develop process actuation systems, to design process schedules and component shape, and to develop a control model with which to control the process.

Keywords

consolidation, finite element method (FEM), hot isostatic pressing, *in situ* sensors, intelligent control, intelligent processing of materials, solidification, vertical Bridgman

1. Introduction

INTELLIGENT processing of materials (IPM) deals with the active control of a material process using analytical or empirical models and *in situ* sensing of critical product features and process parameters to modify process schedules to meet predefined product goals. IPM involves the integration of three enabling technologies: process modeling, *in situ* sensing, and intelligent control. Recently, IPM-based control technologies have been developed for powder consolidation and vertical Bridgman (VB) crystal growth. These technologies typically involve:

- Development, implementation, experimental validation, and application of process models
- Development and installation of *in situ* sensors
- Development and implementation of control algorithms for closed-loop control

Process models include high-fidelity FEM-based models and reduced-order models. The application of FEM-based computational methods to the modeling and control of advanced material processes has been discussed in the literature. FEM-based models are used to predict the time evolutionary behavior during HIP,[1,2] bulk crystal growth,[3] inductively coupled plasma deposition,[4,5] and many other material processes. FEM-based models also can be used to determine optimum process conditions, design the process schedules (such as furnace thermal profile, pressurization, and heating rates), identify critical areas for sensor placement, and assist in the design of process equipment. However, a primary advantage of the FEM-based approach is in the development of real-time feedback control strategies based on the FEM model.

N.M. Wereley, T.F. Zahrah, and **F.H. Charron,** BDM Federal, Inc., 4001 N. Fairfax Dr., Suite 750, Arlington, VA 22203.

*The results in this article were presented at the AeroMat '93 Advanced Aerospace Materials/Processes Conference and Exposition, Anaheim, CA, 7-10 June 1993.

A key parameter dictating the performance of an intelligent control system is the control interval. The control interval is the duration during which all sensor measurements are obtained, model predictions are performed, control algorithms are executed, and commands are sent to the process actuators to effect changes in a process schedule. The control interval typically is selected between 10 and 20% of the fastest time constant of the process. In general, the control interval for a typical advanced material process is much shorter than the time in which an FEM model can be executed to predict the same process behavior. To be included in a model-based control system, the process model must be able to predict process behavior in real-time. This leads to the notion of the reduced-order model, a model that is sufficiently simplified and accurate, to permit real-time prediction.

This fundamental trade-off between high-fidelity models and reduced-order models is explored for consolidation and solidification processes for which IPM systems have been developed by the authors. Near-net shape forming of powder materials using hot isostatic pressing (HIP) required the development of an IPM system to make on-line assessments of how consolidation is proceeding and to take any control actions (changes to the pressure and temperature schedules) needed to return the process to the desired processing path. The IPM system required (1) the development and application of process models for powder consolidation, (2) the use of eddy current sensors to monitor shape change during consolidation, and (3) the development of adaptive proportional + integral + derivative (PID) and model-based intelligent control strategies for consolidation.

The goal of IPM-based directional solidification of CdTe bulk crystal using the VB growth technique is to increase the single crystal yield and to control stoichiometric uniformity. The basic growth process involves relative translation of a quartz ampoule filled with unrefined molten CdTe through a temperature profile that includes its solidification temperature. A prototype industrial VB reactor was designed and assembled, and an IPM system for real-time monitoring and process control of CdTe bulk crystal growth was developed. The IPM system required the development and application of (1) a crystal growth model for conductive, radiative, and convective heat transfer mechanisms in the VB growth system; (2) *in situ* sensors to monitor ingot conductivity, and the shape and location of the solidification front; and (3) adaptive control of material

properties, ingot temperatures, and solidification front shape and location by modifying the thermal profile and/or translation rate of the furnace.

2. Intelligent Control of HIP

The first complete IPM system for HIP has been installed at the Naval Air Warfare Center and it has successfully consolidated metallic and intermetallic powders under closed-loop control to achieve predefined goals. The IPM-based control system required the development of process models, implementation of eddy current sensor technology, and development of intelligent control strategies.

2.1 *Process Modeling*

Although the process of consolidation is continuous, it is helpful to think of consolidation as occurring in three stages. The initial stage, referred to as Stage 0, is dependent on powder size distribution and component shape, as well as several preconsolidation steps, including encapsulation and binder burnout. Consolidation includes two stages. In Stage 1, voids within the material are interconnected, and deformation is concentrated at interparticle contacts. As relative density increases, the interparticle contact area increases until most of the interconnected voids are sealed off. The material, with isolated voids, is now in Stage 2.

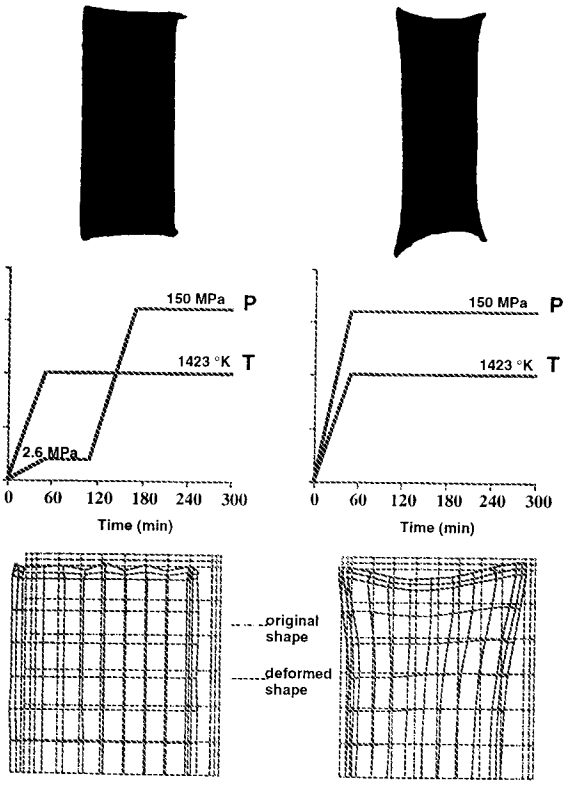

Fig. 1 Results from PROSIM™ are in agreement with experimental observations.

The authors have worked with researchers from Cambridge University, University of California at Santa Barbara, and University of Pennsylvania on the development, implementation, and validation of constitutive models for consolidation of powder materials subjected to three-dimensional stress states.[2,6,7] The micromechanics mechanism-based models have been implemented in a general-purpose finite-element program. The numerical integration scheme uses a rate-dependent formulation to allow coupling of all densification mechanisms, applies to three-dimensional stress states, and allows the use of a coupled heat transfer/stress analysis solution algorithm. This PROcess SIMulation, PROSIM™, computer program can now be used to perform simulation for different process cycles, and the results will identify the active densification mechanism(s) and the contribution of each mechanism to densification.

To illustrate the application of these models to simulate the consolidation process and demonstrate their usefulness, computer simulations of two HIP experiments described by Li, Ashby, and Easterling[8] were performed. In these experiments, steel canisters with torroidal shape were filled with tool steel powder and HIPed under two different temperature and pressure schedules, as illustrated in Fig. 1. Canister deformation or shape change was observed in one experiment, whereas no shape change was observed in the other experiment. The deformed shapes obtained through numerical simulations[1] agree with the experiments, as illustrated in Fig. 1. An examination of the analysis results illustrated in Fig. 2 show that, for the case in which shape change occurred, the plastic yielding mechanism was active early during consolidation. Power-law creep is dominant during the latter stages of consolidation. For the case in which no shape change occurs, power-law creep is the only active mechanism. These results illustrate the importance of process schedule and encapsulation design. Without a canister, no shape change occurs in specimens of this size (about 1 in. in thickness by 2 in. in height). In thick specimens, temperature gradients can result in nonuniform densification

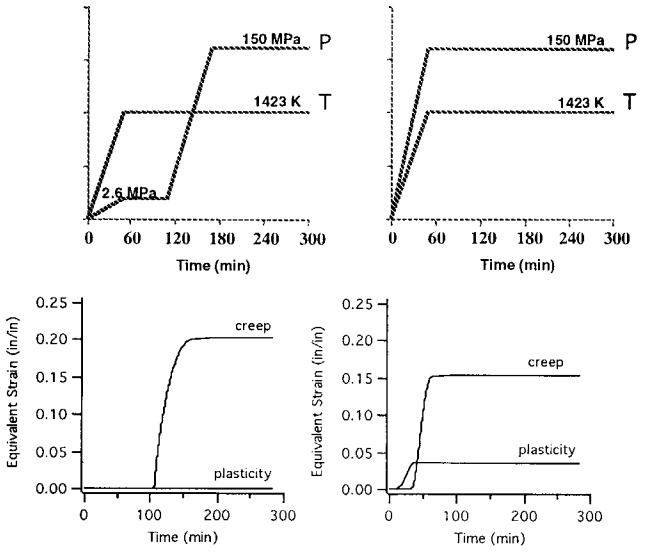

Fig. 2 Contribution of plastic yielding and power-law creep mechanisms to powder densification for the two HIP schedules.

and shape change. The temperature gradients obtained during the computer simulations were less than 10 K. The results explain the source of shape distortion, which is mechanism based, and illustrates the advantage of mechanism-based models. Shape change is the result of the mechanisms that were active during consolidation.

2.2 *In Situ Sensors*

Of crucial importance to the ultimate success of the closed-loop IPM system for HIP is the implementation of *in situ* sensors from which process states can be either directly sensed or inferred. Estimates of sample density are required during HIP to control the consolidation process effectively. Two eddy current sensors were developed to monitor the changes in canister dimension and to provide estimates of part density. The estimates of powder compact density can then be used to adjust process schedules in the event that consolidation is not progressing as expected.

The two types of eddy current sensors are a global (or encircling) sensor and a local (or probe) sensor. Substantial engineering has been performed to harden these two eddy current sensors to survive the hostile environment inside a HIP chamber.

2.2.1 Global Sensor

The global (or encircling) eddy current sensor nondestructively monitors key electrical features of a sample during the HIP process, from which reliable estimates of the sample diameter can be calculated. The global sensor consists of two coils. A primary coil that encircles the HIP sample and to which an electrical excitation or stimulus is applied, and a secondary coil that is concentrically aligned to the interior of the primary coil at the center of the longitudinal axis. The secondary coil picks up an electrical signal, or a response, that is proportional to the diameter of the sample inside the secondary. The resulting stimulus-response pair is used to calculate a frequency-dependent impedance curve. Effects of noise, lead placement, etc., can be eliminated by normalizing this impedance curve with respect to an impedance curve derived from an empty sensor. This temperature-compensated normalized impedance curve is the basic data set used in all of the estimation techniques.

2.2.2 Local Eddy Current Sensor

The local (or probe) eddy current sensor nondestructively monitors key electrical features of a sample during the HIP process, from which reliable estimates of the distance between the sensor and sample can be calculated. The probe sensor also uses a primary and secondary coil configuration, although of a different geometry from the global sensor. The probe sensor has greater flexibility due to the wider variety of possible mounting configurations. Shape features can be measured by appropriately placing sensors around the sample on mechanically and thermally stable mounts.

2.3 *Intelligent Control*

The intelligent control system (ICS) for HIP is a UNIX-based supervisory control and data acquisition (SCADA) system enabling an operator to design, execute, and control HIP process schedules. It consists of three software modules: a process design module, a process control and data acquisition module, and a data analysis module.

The process design module uses PROSIM™ or PDT™ to generate candidate process schedules (process inputs such as temperature and pressure schedules versus time), exercise process models, and predict consolidation. Depending on the component shape and size (which affect the size of the finite-element mesh), PROSIM™ may require more time and computer resources than available on-line during HIP. By assuming a uniform stress state, a reduced-order model suitable for embedding in a real-time control system can be derived. The stress state will vary depending on the consolidation process and part complexity. For HIP of a right circular cylinder, a hydrostatic stress state is the simplifying assumption used to produce a suitable reduced-order model. Reduced-order models for different stress states have been implemented in PDT™, a process design tool.

The process control and data acquisition module executes process schedules developed with PDT™ and/or PROSIM™ and controls processing variables such as temperature and pressure. It executes supervisory control, estimation, and low-level control strategies for HIP. Supervisory control monitors key process parameters, determines if the process goals are achievable, and modifies the process schedules, if required. Estimation provides on-line estimates of key process variables that are not directly measured by *in situ* sensors. Existing estimators use eddy current sensor data to estimate internal temperature fields. Additional estimators are under development to estimate material properties that include yield stress and initial packing density. Low-level control uses control strategies, such as PID and fuzzy logic, to track the process schedules.

The data analysis module provides tools for the analysis and graphical representation of eddy current sensor impedance data collected during processing. Software tools are provided to replay the entire process database, manipulate the data, and create new process schedules for subsequent HIP cycles.

The IPM system provides off-line process planning using either PROSIM™ or PDT™ to produce process schedules consisting of a reference temperature, pressure, and density trajectories. Feedback control techniques are then used to track the reference trajectories, as illustrated in Fig. 3. The objective of the on-line IPM control strategy is to track the reference density trajectory by minimizing density tracking errors. If the measured density undershoots the reference density trajectory, then the controller increases temperature and pressure, which softens the material and increases densification rate. Conversely, if the measured density overshoots the reference density trajectory, then the controller decreases temperature and reduces densification rate. The authority to control the HIP process is shared between an off-line process design and an on-line feedback control strategy.

The IPM system uses PID compensation to track density. PID is a non-model-based control approach, which refers to a control strategy that does not execute a real-time model to determine a control action. After the density tracking error is compensated by the PID controller and checked against HIP equipment constraints, the resulting temperature correction is

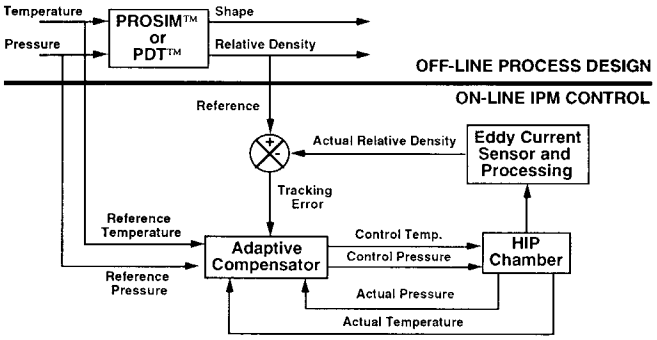

Fig. 3 IPM-based intelligent control system for HIP uses off-line process design and an on-line density tracking IPM control strategy based on reference trajectories for temperature, pressure, and density developed using the process design module, PDT™. Currently, an adaptive gain-scheduled PID algorithm has been implemented. Future implementations will include a linearized LQG model-based compensation technique and a fuzzy logic compensator.

added to the reference temperature. The pressure change is a function of temperature according to a nonideal gas law relationship.

2.4 *Application to a CP Ti Part*

Closed-loop control of density was demonstrated for a 1 in. diameter can of CP Ti (PREP) powder. The HIP cycle was designed to maintain a relatively constant rate of densification from the initial packing density to the desired final density. The off-line process schedule design anticipated data from temperature, pressure, and global eddy current sensors. Relative density was calculated based on diameter estimates obtained from the eddy current sensor. A thermodynamic model of the chamber represented the nonideal argon gas law. The reference temperature, pressure, and density trajectories, illustrated in Fig. 4, were developed using PDT™ in conjunction with the chamber model. Note, however, that the reference pressure trajectory was purposefully designed to be too aggressive for this HIP chamber to emphasize the benefits of feedback control. The basic stages of the HIP cycle were as follows: cold pressurization, heating, temperature soak, and cooling. The HIP cycle starts with a cold pressurization to 36 MPa (5.3 ksi) at 373 K (100 °C), then ramps to 1000 K (727 °C) and a pressure of 75 MPa (11 ksi), and holds for 20 min before finally free cooling. The objective of the closed-loop control system for this HIP run is to track the reference density trajectory shown in Fig. 4.

The closed-loop HIP run was performed using the reference trajectories shown in Fig. 4. The actual (measured) temperature and pressure trajectories were obtained from on-line HIP chamber monitoring. The actual (measured) density trajectory was obtained on-line from the global eddy current sensor. The control trajectory portrays the temperature and pressure set points sent to the PID loops controlling the HIP chamber temperature and pressure. With no density trajectory error feedback, that is, open-loop control, the temperature and pressure control trajectories would be identical to their respective reference trajectories. However, when using feedback control, each control set

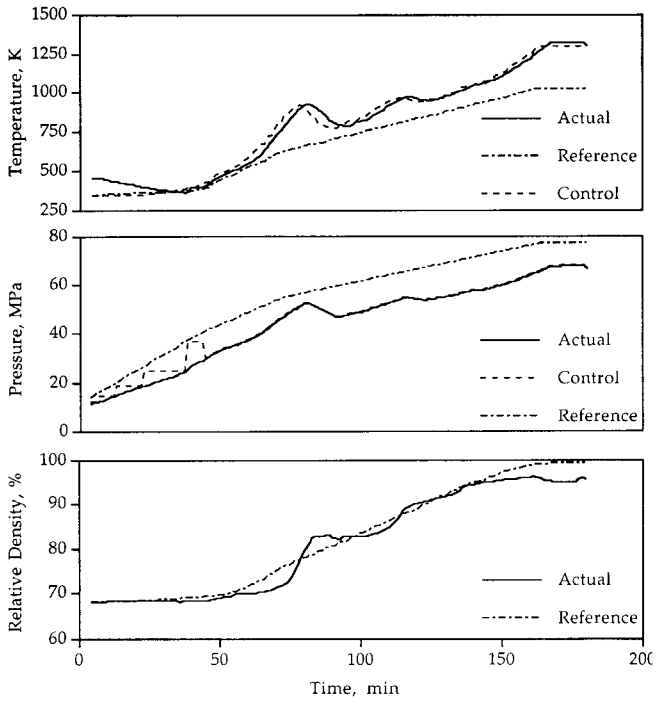

Fig. 4 Closed-loop control of a HIP cycle for CP Ti.

point is determined as a function of the density tracking error. The difference between control and actual trajectories is governed by the pressure (pumping and venting) capability of the HIP chamber.

The PID control strategy provided good density tracking performance for this CP Ti sample. The measured density tracked the reference density quite well, as illustrated in Fig. 4. The first sign of a density tracking error occurred after the cold pressurization portion of the HIP cycle. This tracking error is due to the overly aggressive reference pressure trajectory. The ensuing oscillations in the actual density trajectory are due to a pressure shortfall at the end of cold pressurization, which was compensated by an increase in temperature. If the reference pressure trajectory had been achieved by the HIP chamber, then the reference temperature and pressure trajectories would have produced the reference density trajectory.

2.5 *Model-Based Control*

The FEM model is the model with the most fidelity in terms of accurate prediction of process behavior. To reduce the order of the model, assumptions are made on the process conditions, container shape, and physical properties of the material being HIPed. For example, by assuming a uniform stress state, a suitable reduced order model can be developed and embedded in a real-time, intelligent control system. The stress state will vary depending on the consolidation process and part complexity. For HIP of a right circular cylinder, a hydrostatic stress state is the simplifying assumption used to produce a suitable reduced order model.

To illustrate the application of the uniform stress state assumption, consider the model for Stage 1 power-law creep

mechanism. The full three-dimensional formulation is implemented in PROSIM™. By assuming a uniform hydrostatic stress state, the densification rate for Stage 1 power-law creep mechanism can be described by a nonlinear ordinary differential equation (NLODE).

$$\dot{D}(t) = D(t)C_{cr}(t)P^n$$

where

$$C_{cr}(t) = \frac{27\pi}{16\sqrt{3}} B_{cr} \frac{(1-D_0)^{n-1/2}(D-D_0)^{1/2}}{[3D^2(D-D_0)]^n}$$

$$B_{cr} = \frac{A\mu b}{kT} D_{cr} \left(\frac{1}{\mu}\right)^n$$

$$D_{cr} = D_{0,cr} \exp\left(-\frac{Q_{cr}}{RT}\right)$$

Here, $\dot{D}(t)$ is the densification rate; $D(t)$ is the current relative density; D_0 is the initial relative density; T is the temperature; P is the applied pressure; n is the creep exponent; Q_{cr} is the activation energy for creep; A is Dorn's constant; R is the universal gas constant; k is Boltzmann's constant; μ is the shear modulus of the fully dense material; and b is Burger's vector. These equations can be combined to yield:

$$\dot{D}(t) = 3.1 B_{cr}(T) D \left(\frac{D-D_0}{1-D_0}\right)^{1/2} \left[\left(\frac{1-D_0}{D-D_0}\right)\frac{P}{3D^2}\right]^n$$

Each of the plasticity, creep, and diffusion mechanisms for both Stage 1 and Stage 2 can also be described by an NLODE. The states associated with HIP are density, $D(t)$, and grain size, $G(t)$. The control input variables are temperature, T, and pressure, P. The output variables are given by part temperature T_p, and density, $D(t)$, measured by the eddy current sensor, although additional output variables could be used if *in situ* sensors were available. This model is in the right form to develop a model-based control strategy. One technique for developing a control model is based on linearizing the NLODEs that make up the process model.[9] Essentially, a nominal temperature and pressure trajectory is developed using PROSIM™. The resulting density and grain size trajectories are then calculated, which together with the temperature and pressure trajectories make up the process trajectory. A linearized model describes small perturbations of the nonlinear system about the process trajectory. The NLODEs that comprise the nonlinear model are then transformed to a set of time-varying linear equations, to which standard linear control system design tools can be applied. A gain-scheduled linear quadratic Gaussian control strategy is currently under development and may improve density tracking performance of the HIP control system.

The non-model-based adaptive PID technique invests all control authority in process trajectory specification running off-line. The adaptive PID approach can only mitigate small deviations from the designed process trajectory by tracking the reference density trajectory. This initial approach was taken to minimize the impact of unmodeled dynamics and parameter uncertainty that may have existed at the time the adaptive PID was implemented. As consolidation model validation proceeded, and these sources of error were reduced and/or eliminated, implementation of a model-based control strategy became feasible. Implicit in the model-based technique is the increase in real-time control authority that is implied by introducing a process model and control algorithm running in real-time that can modify the process schedules. The model-based feedback control techniques should be able to deal with much larger deviations from the process trajectory due to sensor noise and other disturbances. The details of this work in progress will be reported in a future article.

3. Intelligent Control of Solidification

The primary objective of the intelligent control system for solidification is to demonstrate model-based, flexible manufacturing for directional solidification of infrared (IR) and other semiconductor materials. To achieve this objective, a prototype vertical Bridgman (VB) reactor was built and tested. The prototype VB reactor was developed using the IPM approach, which combines process modeling and simulation, *in situ* sensors, and adaptive control to achieve significant improvement in crystal producibility and product performance. In this section, some primary results from the first phase of an ARPA-sponsored program are described.

The intelligent VB reactor is intended to be extremely flexible, enabling production of multiple materials (CdTe:In, CdZnTe, InSb, etc.). CdTe materials have been used extensively in infrared electro-optic (EO) modulator applications due to their substantially higher modulation coefficient compared to material systems such as GaAs. However, use of CdTe modulators has been severely restricted due to the extremely low yields of the processes used to produce this family of materials, leading to extremely high price and unpredictability of deliveries. The CdTe family of materials is also used as IR substrates in HgCdTe growth.

The main process control objective is to produce a large single-grain crystal. The primary source of yield loss is in the size of single-crystal material. In this respect alone, this material lends itself to improvement using innovative IPM techniques to predict and control the crystal growth process. Although yield loss is primarily due to the size of single crystals, requirements to provide optimum modulation performance (high electrical resistivity, low absorption at the required wavelength, and resistance to breakdown under an applied electric field) present a challenge to produce material of sufficient quality with repeatability.

Application of IPM to the crystal growth of EO modulator material will improve process yields in two ways: (1) dramatically improve single-crystal yield and (2) control the electro-

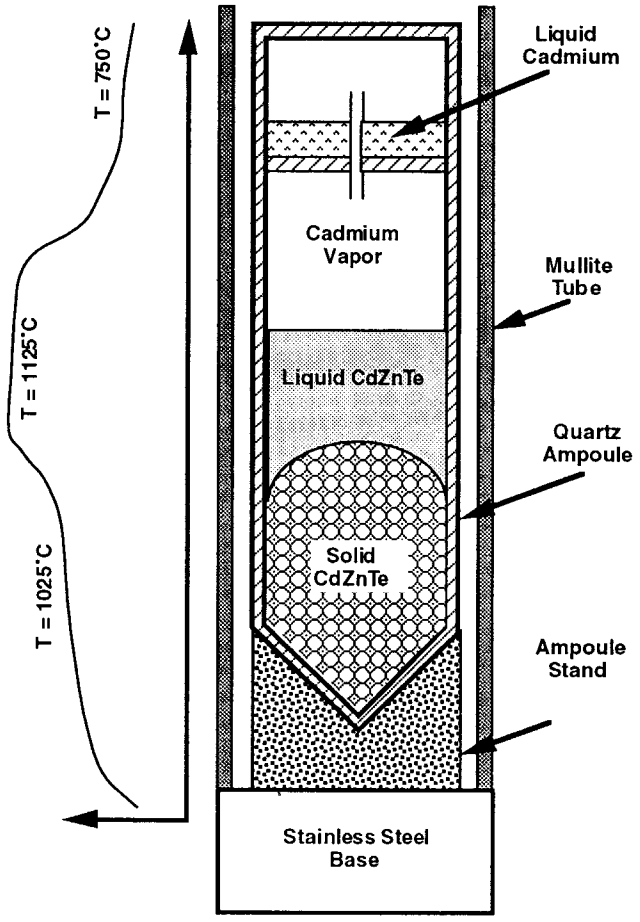

Fig. 5 Schematic of the materials and furnace configuration used to model the vertical Bridgman crystal growth process. A nominal axial thermal profile is illustrated to emphasize heat exchange aspects of the desired process models.

optic properties of the material, especially resistivity, during the growth and cool down phases of the process.

A schematic of the VB crystal growth system is shown in Fig. 5. The basic growth process involves relative translation of a quartz ampoule filled with unrefined molten material (CdTe or CdZnTe) through a temperature profile that includes its solidification temperature. This is done by either translating the furnace relative to the quartz ampoule, or by translating the temperature gradient along the longitudinal axis of the furnace, while holding furnace and ampoule stationary. In the industrial process, the quartz ampoule is stationary and the furnace translates. An important performance objective is to maintain predetermined longitudinal and radial temperature profiles. In some cases, composition of the melt can be controlled through Cd overpressure generated by heating a Cd reservoir in the top of the ampoule (typically to a temperature of around 800 °C).

Three thermal profiles for VB growth are illustrated in Fig. 6. Existing VB reactors typically apply a parabolic thermal profile, as shown on the left. During the initial stages of this effort, a prototype 17-zone VB reactor capable of providing a flat thermal profile in the hot zone of the furnace was built. The gradients, G_1 and G_3, were set before growth. In the advanced VB

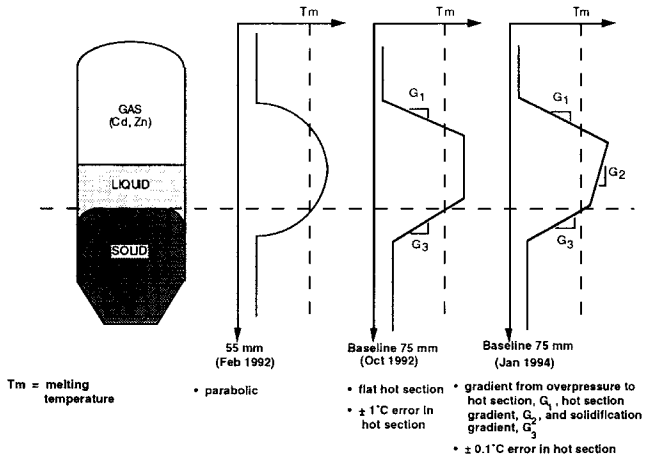

Fig. 6 Advanced thermal profile control. Existing industrial VB furnaces typically use a parabolic thermal profile. An improved industrial furnace design was developed to provide a flat thermal profile in the hot section, as shown in the second thermal profile. Transitioning to advanced thermal profile control will allow direct control of gradients G_1, G_2, and G_3 to vary process parameters that can be used for experimental model verification at minimal cost.

reactor, the thermal profile, shown on the right, will have three gradients (G_1, G_2, and G_3) that can be actively controlled during growth.

The advantages of controlling these three gradients, especially G_3, will be explored. In addition, the use of an FEM process model to develop ampoule stand designs, furnace geometry, and control strategies will be discussed for CdZnTe crystal growth.

3.1 *Process Modeling*

Models for heat transfer, fluid flow, and stress analysis are under development for VB crystal growth. The lack of critical thermophysical properties hinders the accuracy of these models and the use of *in situ* sensors as part of an IPM system. The key thermophysical constants required for proper modeling of VB crystal growth of CdZnTe can be grouped into three categories: thermal properties, physical properties, and optical, electrical, and magnetic properties. Thermal properties are required for analysis of heat transfer and fluid flow. Physical properties are required for stress analysis. Optical, electrical, and magnetic properties of CdZnTe in both the solid and liquid phases are required for *in situ* sensor design.

Good estimates of pertinent physical properties for CdZnTe are necessary for modeling, sensing, and control applications. The property values are needed at both room temperature and at elevated crystal growth temperatures. At present, the published data set is incomplete, and most of the published properties are limited to room temperature.

Models used for analysis of VB crystal growth need to account for heat transfer and fluid flow and must be able to calculate the stresses induced in the ingot. ABAQUS, a general-purpose finite-element code, was chosen to model heat transfer, including conductivity and radiation, and stress analy-

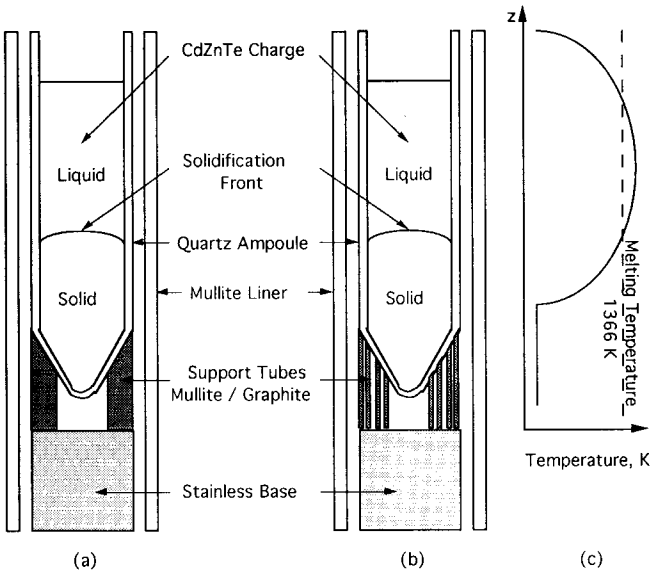

Fig. 7 Vertical Bridgman crystal growth reactor configuration. (a) Ampoule stand is a solid thick-walled tube fabricated from either mullite or graphite. (b) Ampoule stand is a series of four thin-walled tubes fabricated from either mullite or graphite. (c) Nominal parabolic thermal profile used to evaluate performance of the ampoule stand configurations.

sis. The results are used to provide a better understanding of the heat transfer problem and to predict the shape and location of the solidification front.

3.2 *Ampoule Stand Design*

First, the current industrial VB system (Fig. 7) was analyzed with the parabolic thermal profile. In these calculations, the ampoule diameter was 55 mm. The VB configuration is axisymmetric, with the axis of symmetry corresponding to the axis of revolution of the ampoule. As a result, the VB geometry can be modeled exactly using axisymmetric elements. Eight-noded, axisymmetric quadrilateral elements were used to generate the mesh. The mesh includes elements describing the mullite sleeve, quartz ampoule, CdZnTe mixture, ampoule stand, and stainless steel base. The model includes algorithms for calculating radiative heat exchange between the quartz and mullite and the thermal interaction between the furnace and the mullite.

The calculations were aimed at supporting design of the ampoule stand. Key issues were identified, and their effect on the shape and location of the solidification front were examined. The first key issue examined was the design of the ampoule stand, including geometry and thermal conductivity of the material. The ampoule stand was assumed to be a solid thick-walled tube, as in Fig. 7(a), or four concentric thin-walled tubes as illustrated in Fig. 7(b). The inner diameter of the central open core was assumed to be the same in both cases. The material choices for the ampoule stand were mullite (low-conductivity material) or graphite (high-conductivity material). For these calculations, the furnace temperature profile was assumed to be parabolic, as illustrated in Fig. 7(c). This temperature profile was used to define the thermal boundary condition at the outer surface of the mullite furnace liner.

To illustrate the effects of ampoule stand material and geometry, the thermal profile was positioned such that the CdZnTe melting temperature was within the conical base of the ampoule. The isotherms for this case are illustrated in Fig. 8. The steady-state heat transfer solution algorithm was used. The results provide the temperature distribution within the ampoule and support structure. The isotherm at the melting temperature (1366 K) gives the shape and location of the solidification front. Based on the results, the shape and location of the solidification front are strongly dependent on the choice of ampoule stand material and weakly dependent on geometry of the ampoule stand.

Additional calculations were performed with the melting temperature at different locations inside the ampoule. The shape of the solidification front is nearly flat for an ampoule stand with low thermal conductivity (mullite) and highly convex for an ampoule stand with high thermal conductivity (graphite).

The location of the solidification front is in the same horizontal plane as the location of the CdZnTe melting temperature in the furnace temperature profile for an ampoule stand with low thermal conductivity material (mullite) and higher than the location of CdZnTe melting temperature in the furnace temperature profile for an ampoule stand with high thermal conductivity material (graphite). This implies that a thermocouple measurement of the furnace liner is a poor indication of temperature inside the ingot.

The ampoule stand material greatly affects the shape and location of the solidification front when the melting temperature in the furnace temperature profile is within the conical base of the ampoule. The effects diminish as the melting temperature moves into the cylindrical part of the ampoule.

3.3 *Evaluation of Furnace Design*

Following these initial findings, additional calculations were performed to support prototype furnace design. The prototype is a set of three Marshall-type furnaces, mounted on a stepper motor-driven vertical translation table, as illustrated in Fig. 9(a). The ampoule diameter used in the prototype furnace was increased to 75 mm. The temperature profile of the prototype furnace consists of three segments, as illustrated in Fig. 9(b). Two segments have a constant temperature, one segment below the melting temperature (cold section) and the other above the melting temperature (hot section). The thermal profile was maintained constant in the hot region to minimize convection. The third segment is a linear transition through the melting temperature, denoted by G_3. This temperature gradient, G_3, is the key process parameter to be evaluated in this analysis. Calculations were performed for five temperature gradients, namely, G_3 = 4, 8, 12, 16, and 20 K/cm. Because the dependency of solidification front shape on ampoule stand geometry is weak, only the thick-walled tube ampoule stand results are shown in Fig. 10. The material of the ampoule stand was assumed to be mullite, which has a low thermal conductivity compared to graphite. The results for graphite are not shown.

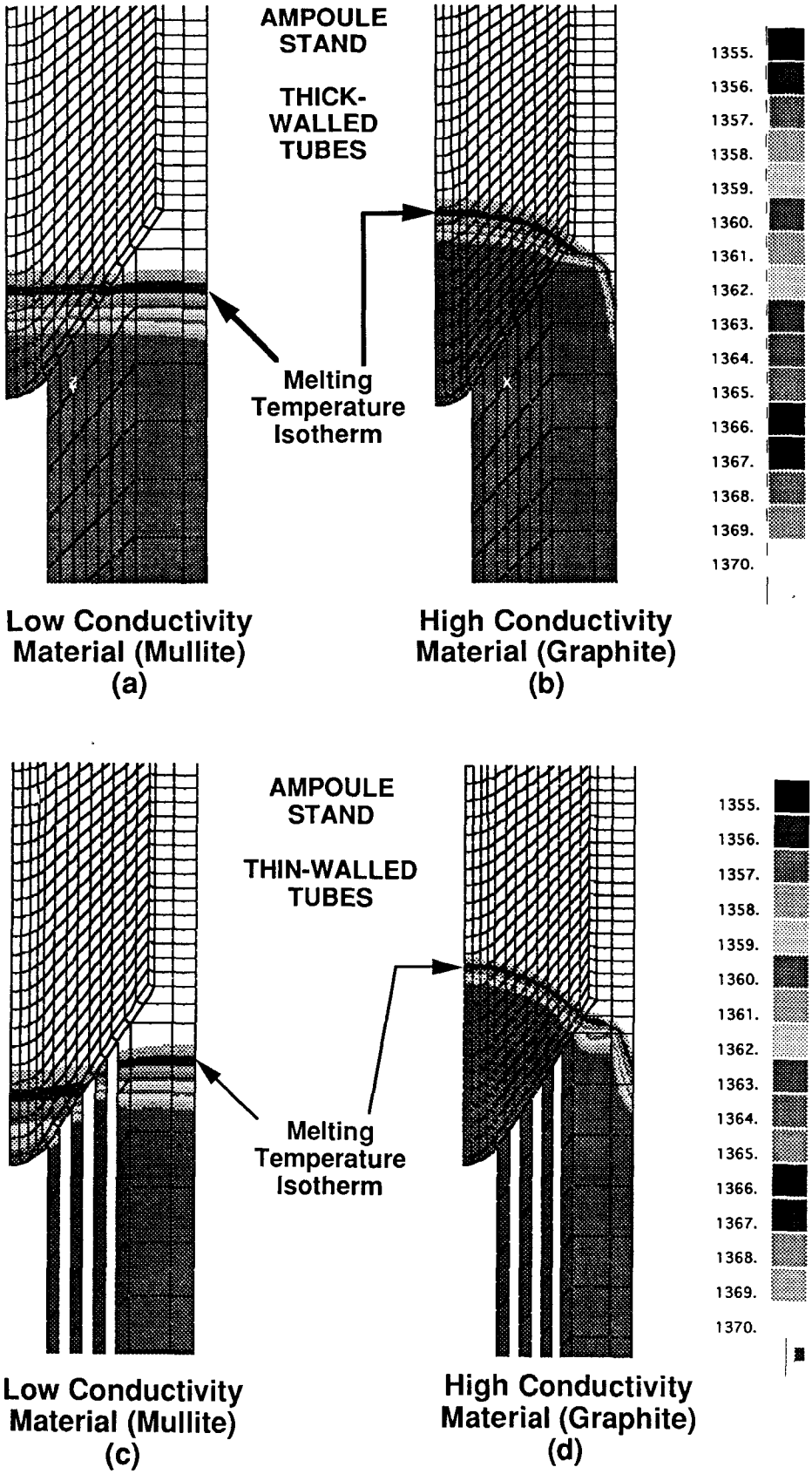

Fig. 8 Isotherms for vertical Bridgman configuration with melting temperature positioned within conical base of ampoule. Results show that solidification front curvature is strongly dependent on ampoule stand material and weakly dependent on ampoule stand geometry. (a) Ampoule stand is a thick-walled mullite tube. (b) Ampoule stand is a thick-walled graphite tube. (c) Ampoule stand is a series of thin-walled mullite tubes. (d) Ampoule stand is a series of thin-walled graphite tubes.

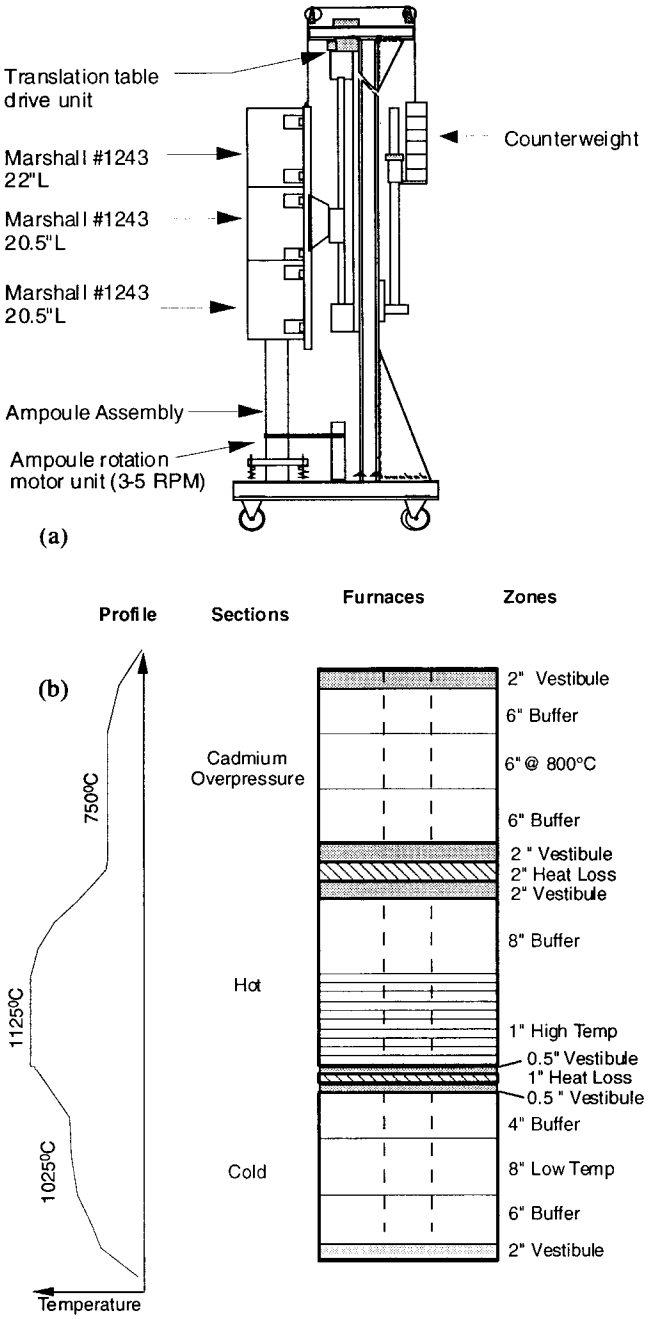

Fig. 9 Prototype vertical Bridgman reactor configuration.

Several positions of the furnace were considered. The corner of the ampoule is the location where the straight vertical line representing the ampoule wall transitions to the slanted wall of the conical ampoule bottom. A value of $z = 0$ denotes a position where the melt point in the temperature gradient, G_3, is coincident with the ampoule corner. Positive values of z are upward. Several values of z were considered, i.e., –4 cm, –2 cm, 0 cm, 2 cm, and 4 cm. The isotherm at the melting temperature (1366 K or 1093 °C) of CdZnTe gives the shape and location of the solidification front. A representative set of isotherms are shown in Fig. 10 for G_3 = 4 K/cm, 8 K/cm, 16 K/cm, and 20 K/cm for a position of $z = 0$. For G_3 = 4 K/cm, the solidification front is concave. As the gradient increases, the solidification front shape transitions through flat to increasing convexity, until convexity reaches a maximum for G_3 = 20 K/cm. A larger gradient, if practically feasible, could further increase the convexity of the solidification front.

Based on these results, an increase in ampoule diameter and a change in temperature profile from parabolic to linear combine to reduce the convexity of the solidification front. For an ampoule stand with low thermal conductivity, an increase in the temperature gradient from 4 to 20 K/cm causes the solidification front to transition from slightly concave to flat to slightly convex. For an ampoule stand with high thermal conductivity, an increase in the temperature gradient from 4 to 20 K/cm causes the solidification front to transition from nearly flat to slightly convex. Thus, by changing the applied gradient, the shape of the solidification front can be controlled. This is consistent with other research for horizontal Bridgman crystal growth.[10]

In some cases, the shape of the isotherms at the melting point exhibits waviness. A refined mesh is required for higher resolution of the solidification front shape. The model for concentric thin-walled tubes does not presently allow for radiation between the tubes. These refinements will be included in the model once the design of the advanced prototype is frozen.

The process model developed in this study does not include convective coupling between the mullite sleeve and quartz ampoule. This effect appears to be small, but is a subject for future investigations. The results reported here are in line with experimental observations during baseline crystal growth. Model validation will continue as *in situ* sensor data become available. Once an *in situ* sensor is available for integration in the furnace, the modeling results will support the decision on the location of the sensor near the solidification front.

3.4 *Intelligent Control*

One of the key control objectives in this process is the control of the solidification front shape and location. Here, the approach that is currently under development is described. The convexity of the solidification front is strongly dependent on the thermal gradient, G_3, as illustrated in Fig. 11. The Marshall-type furnace is a resistive coil surrounded by a substantial amount of insulation, that is, a furnace with a very high thermal inertia, and cannot lose heat. As a result, the prototype furnace is very robust, but has poor controllability characteristics. By using a furnace with a low thermal inertia, the gradients in the furnace can be modified during growth.

The parameter Δz, shown in Fig. 11(a), is defined as the vertical distance at the center of the ingot from the location of the melt temperature at the ampoule wall to the melt temperature location at the center of the ingot. If Δz is positive, then the solidification front is convex as seen from the melt zone. If Δz is negative, then the solidification front is concave. A flat solidification front corresponds to $\Delta z = 0$. The results summarized in Fig. 11(b) show the dependence of solidification front convexity, as expressed by Δz, on the location of the melting point in the thermal profile with respect to the ampoule and thermal gra-

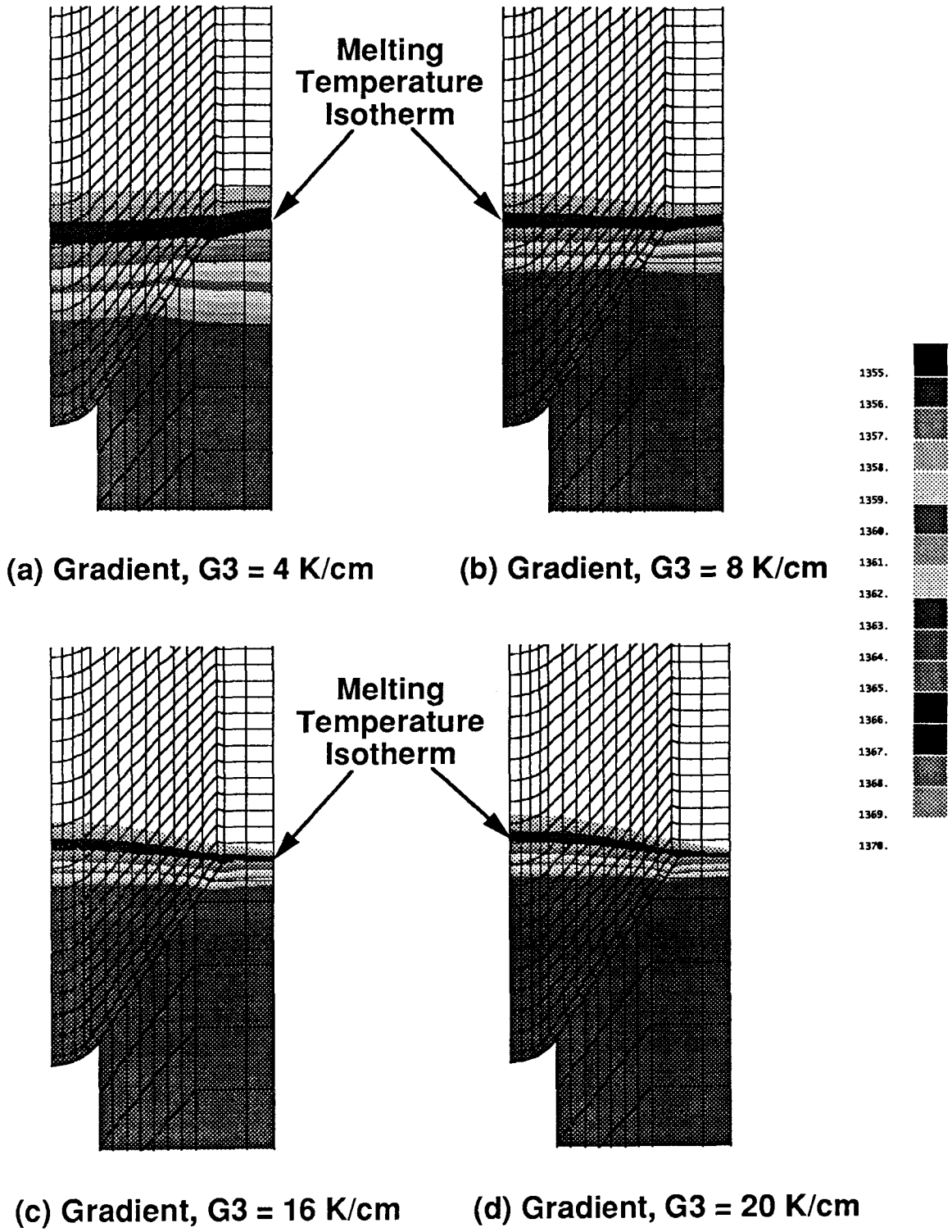

Fig. 10 Isotherms for a vertical Bridgman configuration with a solid thick-walled ampoule stand and a melting temperature positioned at top of the conical base of the ampoule ($z = 0$). Four different values of temperature gradient, G_3, are shown.

dient, G_3. Based on preliminary stress analysis calculations, the parameter Δz is related to the stress field. If Δz is too high, then the stresses in the solid may become greater than the critically resolved shear stress and cause dislocations in the crystal lattice structure. If Δz is too low, then the heat transfer characteristics have become unfavorable, indicating that the heat flux through the ampoule bottom is too low to maintain a convex solidification front.

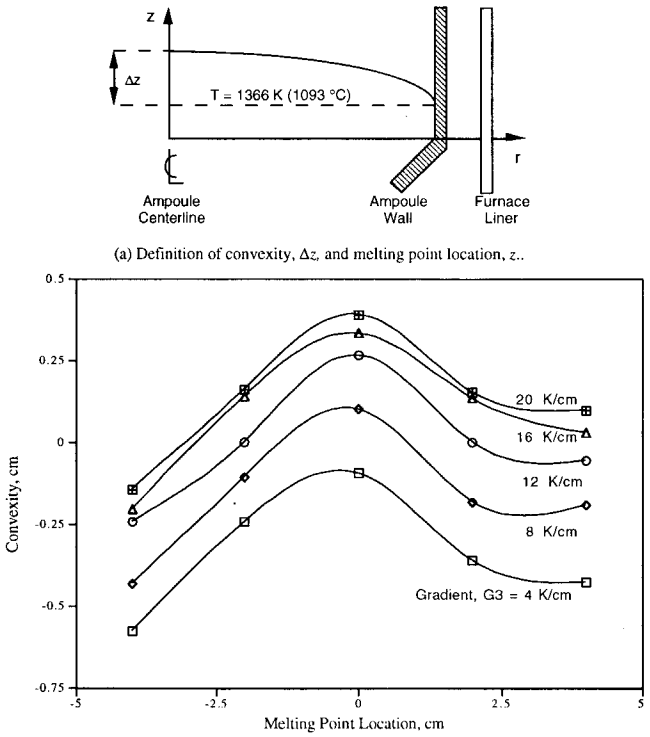

Fig. 11 Operating curves for solidification front shape control. (a) Definition of convexity, Δz, and melting point location, z. (b) Trajectories for solidification front shape control showing convexity, Δz, versus melting point location for different values of the thermal gradient, G_3. Control of solidification front location is achieved through thermal profile position.

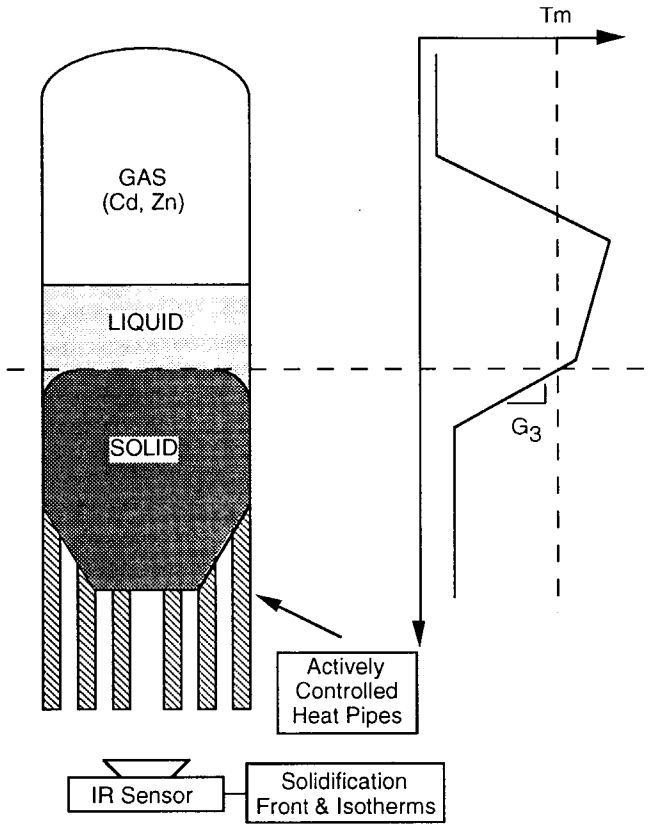

Fig. 12 IR sensor (camera), telescopic zoom lens with short depth of field and imaging software can be used to detect isotherms inside solidifying boule, as well as solidification front shape and location. This technique exploits the axisymmetry of the vertical Bridgman reactor.

Therefore, one control strategy is to select a trajectory for Δz as a function of z based on a stress analysis calculation that minimizes the amount of material exposed to stress fields higher than the critically resolved shear stress and maintains that value of Δz during growth. The reduced-order model is then the curve relating gradient, G_3, to the location of the melting temperature at the furnace liner to maintain Δz (z).

The operating curves in Fig. 11(b) provide some rules of thumb in designing such a trajectory using the mullite thick-walled ampoule stand. The solidification front will be concave for $z < -2$ cm unless a large temperature gradient is used ($G_3 >$ 13 K/cm). Second, for $z > -2$ cm, a temperature gradient, $G_3 \geq$ 8 K/cm, must be maintained, because a flat interface is developed for $z = 0$ and $G_3 = 8$ K/cm, and the curves flatten after $z =$ 2 cm. Larger values of G_3 would be much more favorable for a convex solidification front. Interestingly, the choice of ampoule stand material with a larger value of conductivity would increase the range of z where a convex solidification front occurs, thereby improving the controllability of the solidification front control strategy.

An IPM system to control solidification front shape and location, as illustrated in Fig. 12, is under development. The feedback control loop involves using an IR radiometer (camera) with a telescopic zoom lens with short depth of field and imaging software to detect the shape and location of the solidification front and to map isotherms throughout the solidifying boule. The curvature detected using the IR sensor is then used, in conjunction with the operating curves, to select the appropriate gradient to apply to the crystal growth system.

A second control strategy is suggested by these results. To improve the chance of higher single crystal yield, it makes sense to grow the crystal until solid about halfway up the cone and then arrest furnace translation. Because the solidification front is highly concave below $z = -2$ cm, polycrystalline material may tend to form. Stopping at $z = -2$ cm, holding, and then restarting growth with a large thermal gradient, $G_3 > 12$ K/cm, will tend to produce conditions favorable for a convex interface and a better chance of growing single crystal material. This melt back technique, as suggested by these analyses, is currently being used by an industrial crystal grower.

The impact of material selection on controllability of the solidification front control strategy and the impact of ampoule shape on solidification front shape is currently being studied.

4. Conclusions

Two techniques are discussed for generating a reduced-order control model from a high-fidelity FEM-based model. One consists of simplifying assumption based on the physics of the

problem, and the other discovering a key process parameter and developing a set of operating curves that can be embedded in a model-based controller.

4.1 *Intelligent Control of Consolidation*

Development of an IPM-based intelligent control system (ICS) for HIP relies heavily on a process model, PROSIM™, that accounts for consolidation mechanisms and their coupling, canister deformation, powder packing nonuniformities, temperature gradients within the specimen, and coupled thermal/mechanical behavior. Computer simulations and actual experiments show good agreement for a number of components. PROSIM ™ can be used to design and optimize process schedules to meet predefined goals, such as final shape, relative density distribution, minimization of density gradients, and minimization of residual stresses. The ICS uses a reduced-order process model, PDT ™, for process planning and on-line prediction of process behavior. The assumption of a uniform stress state was used to develop a reduced-order consolidation model for HIP. There are plans to transition this model to fill the role of a real-time control model as the basis for a gain-scheduled linearized LQG control strategy.

4.2 *Intelligent Control of Solidification*

FEM-based models incorporating conductive, convective, and radiative heat transfer, as well as stress analysis, were used to improve the vertical Bridgman CdZnTe crystal growth process. Guidelines for the fabrication of ampoule stands, furnace geometry, and solidification front control strategies were developed using the process model. The models can be used to minimize stresses induced by the thermal environment, as well as tailoring the thermal environment to achieve improved solidification front characteristics. The solidification front control strategy is based on a set of operating curves, or table, describing the effect of changing thermal gradient on solidification front curvature.

Acknowledgments

This work was supported by the Advanced Research Projects Agency (ARPA) under Naval Air Warfare Center (NAWC) contract N62269-91-C-0247, supervised by W. Barker (ARPA) and monitored by Dr. W. Frazier (NAWC), by ARPA contract MDA972-91-0046 supervised by Mr. Ray Balcerak (ARPA), and by internal research and development funds of BDM Federal, Inc.

References

1. T.F. Zahrah, C.J. Coe, and F.H. Charron, The Role of Process Models in Intelligent Hot Isostatic Pressing of Powder Materials, in *Applications and Material Models to Design and Processing*, TMS, Mar 4-5, 1992
2. T.F. Zahrah, N.M. Wereley, F.H. Charron, and J.R. Mills, Hot Isostatic Pressing Using the Intelligent Processing of Materials Approach, in *Proc. Hot Isostatic Pressing '93 Congress*, Elsevier Science Publishers, Antwerp, Belgium, Apr 21-23, 1993
3. N.M. Wereley and T.F. Zahrah, "Infrared Materials Producibility," Final Subcontract Progress Report No. BDM/VAS-0790-TR-93, prepared by BDM Federal Inc. under ARPA contract MDA972-91-C-0046, May 1993
4. D.Y. Wei, D. Apelian, and B. Farouk, Particle Melting in High Temperature Supersonic Low Pressure Plasma Jets, *Metall. Trans. B*, Vol 20, 1989, p 251-262
5. D.G. Backman, E.S. Russell, D.Y. Wei, and Y. Pang, Intelligent Processing for Metal Matrix Composites, *Intelligent Processing of Materials*, H.N.G. Wadley and W.E. Eckhart, Jr., Ed., The Minerals, Metals, and Materials Society, 1990, p 17-39
6. L.T. Kuhn and R.M. McMeeking, Constitutive Models for Powder Compaction Under Non-Hydrostatic Stress States, Report prepared by University of Santa Barbara for BDM Federal Inc., Dec 1991
7. S.M. Govindarajan, "Deformation Processing of Porous Metals," Ph.D. thesis, University of Pennsylvania, Dept. of Mechanical Engineering and Applied Mechanics, Dec 1992
8. W.P. Li, M.F. Ashby, and K.E. Easterling, On Densification and Shape-Change During Hot Isostatic Pressing, *Acta Metall.*, Vol 35 (No. 2), 1987, p 2831-2842
9. N.M. Wereley and T.F. Zahrah, "Linearization of the Consolidation Process Model Using a Uniform Stress State Assumption," Technical Memo BDM/VAS-NMW-draft-93, Jan 1993
10. J.A. Dantzig and L.S. Chao, Interface Shape Control in Bridgman Crystal Growth, *Modeling of Casting, Welding, and Advanced Solidification Processes V*, M. Rappaz, M.R. Ozgu, and K.W. Mahin, Ed., The Minerals, Metals, and Materials Society, 1991, p 715-723